

## Research Article

# Effect of the CHS on Seismic Responses of the Single-Layer Spherical Reticulated Shell under Vertical Seismic Motions

Jie Xu,<sup>1</sup> Renjie Liu ,<sup>2</sup> Ce Ji,<sup>2</sup> Chao Wang,<sup>2</sup> and Guangyong Wang<sup>2</sup>

<sup>1</sup>School of Civil Engineering, Shandong Jianzhu University, Jinan 250101, China

<sup>2</sup>School of Civil Engineering, Yantai University, Yantai 264005, China

Correspondence should be addressed to Renjie Liu; [renjie.liu@ytu.edu.cn](mailto:renjie.liu@ytu.edu.cn)

Received 12 November 2022; Revised 29 January 2023; Accepted 7 February 2023; Published 22 February 2023

Academic Editor: Tzu-Kang Lin

Copyright © 2023 Jie Xu et al. This is an open access article distributed under the Creative Commons Attribution License, which permits unrestricted use, distribution, and reproduction in any medium, provided the original work is properly cited.

Single-layer spherical reticulated shells are typical roof structures for the gymnasiums. The center-hung scoreboard (CHS) is large weight display device which is usually suspended on the roof of the gymnasium. The effect of the CHS on the dynamic characteristics and seismic responses of the single-layer spherical reticulated shell (SPRS) is not fully clear. In this paper, the effect of the CHS on the SPRS under vertical seismic action is investigated. Two kinds of FE models are built with Abaqus software, including the flexibly suspended model and the simplified model. In a simplified model, the CHS is simplified as four fixed masses on the four CHS suspension nodes. The dynamic explicit method is used for the seismic responses, and the Lanczos method is used for the dynamic characteristics. The influence of the CHS weight and the sling length of on dynamic characteristics and seismic responses are analysed. It turns out that in the flexibly suspended model, the first three vibration modes are free swing of the CHS, and the CHS weight and the sling length have a significant impact on the fourth and subsequent modes. The length of the sling has a large impact on some low-order frequencies, but has little impact on the high-order frequencies. Compared with the simplified model, the axial forces of some structural members and some nodal acceleration in the flexibly suspended model under vertical seismic motions would increase by as high as 523% and 564%, respectively. It turns out that the seismic responses of the SPRS would be underestimated if a simplified model is used for analysis. The region in the central of the SPRS, the hoop members of the SPRS, and the support platform are the most affected regions in terms of both axial force and nodal acceleration.

## 1. Introduction

The single-layer spherical reticulated shell (SPRS) is a typical structural form of long span spatial structure, which has the characteristic of good economy, stability, and seismic behavior. The SPRS is commonly used in large-scale public buildings, and is often used as temporary disaster shelters [1]. At present, the seismic performance of SPRS has been systematically studied [2]. However, the effect of the center-hung scoreboard on the seismic responses of the SPRS has been ignored in most studies.

The research on seismic response of the SPRS has reached many achievements. Cao and Zhang analysed the seismic response of a SPRS and discussed the influence of spans, rise-to-span ratios on the seismic responses in the elastic range [3]. Lin et al. applied the pseudoexcitation

method to analyse the seismic response of reticulated shells in the elastic stage [4]. Shen and Zhi concerned the nonlinear response and studied failure mechanisms under severe earthquakes, and classified failure modes of the single-layer reticulated shells [5]. Considering the material nonlinearity and geometric nonlinearity, Ishikawa et al. [6–8] systematically investigated the seismic response of the SPRSs. The overall stability and collapse mechanism of the SPRSs under earthquake action were discussed in detail. The research results provide a reference for the seismic design of the actual SPRSs. Xue et al. summarized development and progress in seismic design methods and analysis methods for long span spatial structures [9] in the past 30 years.

Investigation on influence factors of the seismic response of the SPRSs has many achievements. Fan et al. studied the seismic response of the SPRSs with semirigid joints [10, 11].

Wang and Shen investigated the stability of reticulated shell structures in practical engineering by using finite element analysis technology [12]. Du et al. considered the influence of damage accumulation effect on the dynamic stability of the SPRS [13]. Zhang et al. conducted incremental dynamic analysis on the SPRS and found that roof quality, rise-span ratio, and span have non-negligible effects on the seismic response [14]. Zhong et al. studied nine reticulated shells under 40 far-field and near-field ground motions and found that near-field ground motions caused more serious damage [15]. Yu et al. found that the effect of supporting flexibility significantly influences the failure characteristics of the SPRSs subjected to severe earthquakes [16]. Zhang et al. [17, 18] studied the effects of different initial geometric defect modes on the seismic performance of the SPRSs. In terms of structural design for engineering, neglect of spatial variation of ground motions would underestimate seismic response of spatial space truss structures [19]. But one-dimensional seismic input is often used in academic research for revealing the deep mechanism of seismic response.

In recent years, researchers showed concern on the influence of roofing system and hanging devices on the seismic response of long span spatial structures. Cao et al. [2] investigated the influence of metal roof panels on the seismic performance of reticulated shells and confirmed that the seismic failure load decreased after the roof panels were considered. Zhou et al. [20] conducted shaking table tests and found that the skin effect of roofing systems could reduce node acceleration response. Huo et al. [21] analysed influence of the roofing system on the seismic performance of the SPRSs, and the results show that the roofing system could greatly change the seismic response and failure under strong earthquake conditions. There are some common nonstructural components in large-span spatial structures, such as catwalks, air ducts, lamps, large screens, suspended ceilings, and other roof pendants. Cai et al. transformed them into suspended mass pendulums to control the vibration response of large-span spatial structures [22]. In the past decade, with the development of professional sports events and other activities, the number of center-hung scoreboard (CHS) applications has increased significantly [23]. The CHS is a large display device hanging in the center of the roof structure, and the heaviest CHS is about 55 t [24]. Xue et al. conducted a shaking table test on a 94 m suspended structure with a 30 t CHS and found that the CHS made a great increase on axial forces and node acceleration under seismic motions [25, 26]. Liu et al. [19] analysed the influence of the CHS on natural dynamic characteristics of space truss structures, and found that the influence on the dynamic characteristics cannot be ignored, especially for low-number frequencies and mode shapes. However, research achievements considering the influence of the CHS on the seismic response of the SPRSs are not enough in current references.

In this paper, the influence of the CHS on the seismic response of the SPRS under vertical seismic motion is investigated. The flexibly suspended models and the simplified models are built in Abaqus software, respectively. Dynamic

characteristics are analysed by the Lanczos method [27], and seismic response is analysed by the dynamic explicit method. The dynamic characteristics and seismic response of the flexibly suspended models and the simplified models are compared and discussed. The influence of the weight and the sling length of the CHS on the dynamic characteristics and seismic response of the SPRS under vertical seismic motion are analysed.

## 2. Models and Methods

**2.1. FE Models.** A long span roof structure uses a single-layer spherical K6 reticulated shell with a diameter of 60 m and a rise-span ratio of 1/6, as shown in Figure 1. The CHS is supported by a support platform, as shown in Figure 2. The support platform and the shell are connected by vertical rods. The CHS and the support platform are connected by slings, and the vertical location of the CHS can be controlled by a hoist system. The slings are made of high vanadium coated cables and other members of the structure are made of steel Q355B. The strain-stress curve of the Q355B steel is shown in Figure 3. Abaqus software is used to establish the FE model, the B31 beam element is used for lattice shell members and platform members, and the T3D2 truss element is used for slings. The B31 is a 2-node beam element with linear interpolation formulations in three-dimensional space. This element allows for transverse shear deformation [28]. The T3D2 is a two-node, 3-dimensional truss element used in two and three dimensions to model slender, line-like structures that support only axial loading along the element [29]. Section specifications of the structural members are shown in Table 1, Figures 2 and 4.

Similar to the mass pendulum, the sling length and the weight of the CHS are the main parameters that affect dynamic characteristics, different sling lengths and different weights are designed to study influence laws. In practice, a safety distance of about 1.0 m is reserved between the CHS and the support platform, and a sling length is selected every 0.5 m among 1.0 m and 9.0 m. The length of the sling is taken as 0.0 m when the CHS is simplified as fixed masses on the suspension nodes on the support platform. Since most of the CHSs used in recent years exceed 20 t and the heaviest ones have exceeded 55 t [23, 24], the weight is selected every 5 t among 20 t and 60 t.

The standard value of dead load  $D$  includes the standard value of uniformly distributed dead load on the roof, which is  $1.0 \text{ kN/m}^2$  and the self-weight of members and nodes. The standard value of uniformly distributed live load on the roof  $L$  is taken as  $0.5 \text{ kN/m}^2$ , and the representative value of gravity load is  $1.0D + 0.5L$ . The boundary conditions are assumed to be three-way fixed hinge supports, see Figure 2. The representative value of gravity load of the roof without the CHS is about 500 t. The weight of the CHS among 20 t and 60 t is about 1/15 to 1/9 of the representative value of gravity load of the roof.

**2.2. Analysis Methods.** Lanczos method is a common method for extracting eigenvalues of space grid structures [27]. The Lanczos method is a very powerful and fast

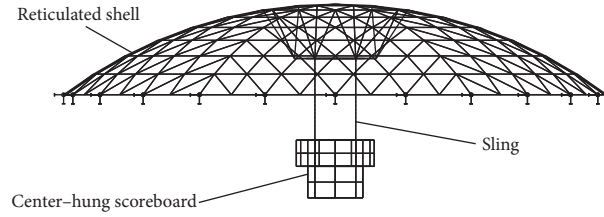


FIGURE 1: Front view of the integrated model.

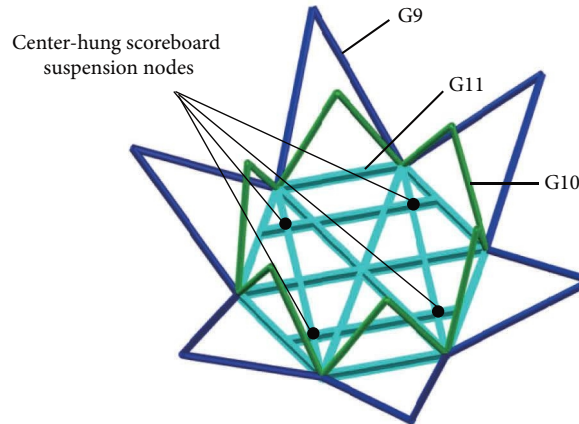


FIGURE 2: The support platform for the CHS.

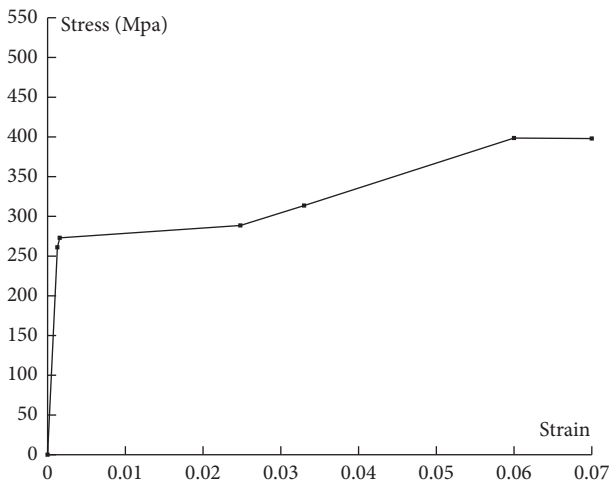


FIGURE 3: Stress-strain curve of steel Q355B.

TABLE 1: Section specifications of structural members.

Section number	Section specifications	Materials
G1	$\phi 273 \times 12$	Q355B
G2	$\phi 273 \times 14$	
G3	$\phi 245 \times 14$	
G4	$\phi 245 \times 12$	
G5	$\phi 230 \times 12$	
G6	$\phi 219 \times 12$	
G7	$\phi 219 \times 10$	
G8	$\phi 325 \times 16$	
G9	$\phi 273 \times 10$	
G10	$\phi 245 \times 10$	
G11	HN550 $\times$ 200	
S1	$\phi 12$	High vanadium coated cable

The section specification of circular pipe  $\phi 245 \times 10$  means the outer diameter is 245 mm and the thickness is 10 mm. The section specification of spiral strand  $\phi 12$  means the nominal diameter is 12 mm.

convergence tool for extracting some of the extreme eigenvalues of real symmetric matrixes, which usually employs a sequence of Krylov subspaces  $\mathbf{K}^1, \mathbf{K}^2, \dots, \mathbf{K}^m$ , and computes Ritz pairs from each other or some of the subspaces [30]. In this paper, the Lanczos method is used to analyse the dynamic characteristics. Commonly used seismic response analysis methods for large-span spatial structures include mode shape decomposition response spectrum method, time history analysis method, and simplified analysis method provided by the regulations [31]. The time history analysis method is a direct dynamic analysis method, which can analyse both the linear elastic

dynamic response and the elastic-plastic dynamic response [32]. In the flexibly suspended model, the CHS is hanging by only-tension slings, the model is a mechanism, and the overall stiffness matrix is singular. Therefore, the dynamic explicit analysis in the Abaqus software is used for calculating the seismic response. For the explicit algorithm, the convergence of the analysis is no problem. The numerical method above has been verified by shaking table test on a suspen-dome structure with a CHS [25, 26], and the accuracy of the numerical results was acceptable if the structure was meshed according to the grid size.

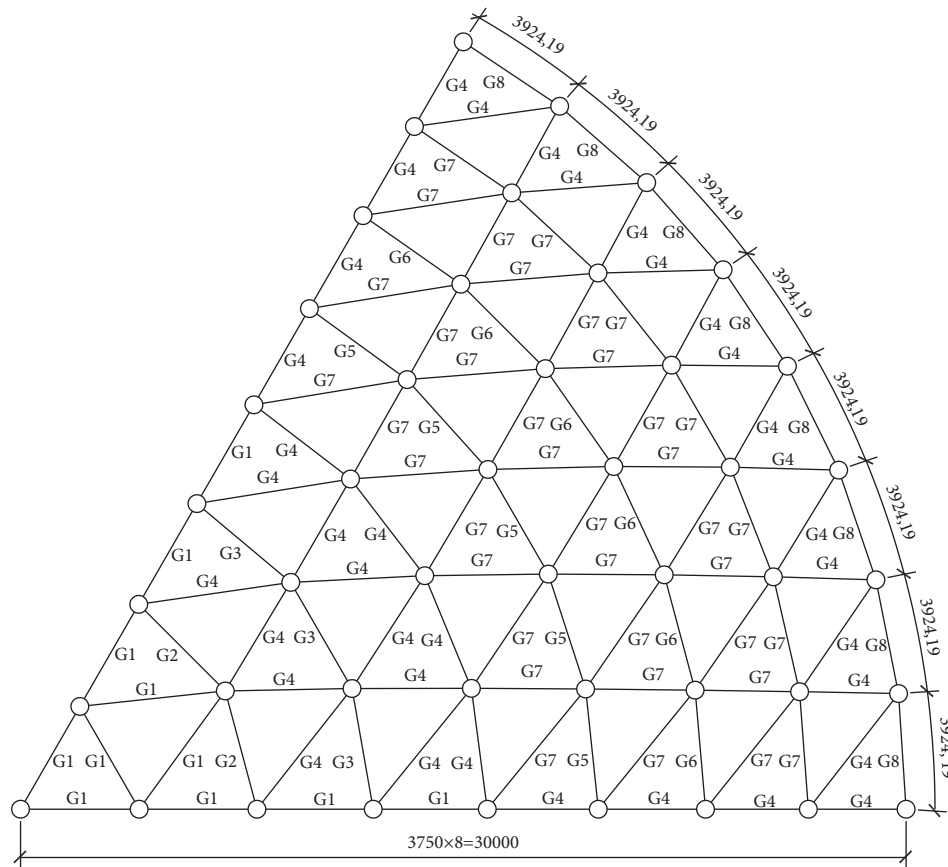


FIGURE 4: The layout of the shell members.

**2.3. Seismic Motions.** In general, the seismic waves available for structural time history analysis include actual seismic records of the proposed site, typical past seismic records, and artificial seismic waves. According to provisions of the regulation [32], when the time history analysis method is used, the actual strong earthquake records and the artificially simulated acceleration time history curve should be selected according to the type of construction site and the design earthquake group, and the number of actual strong earthquake records should not be less than 2/3 of the total number, the average seismic influence coefficient curve of multiple sets of time history curves should be consistent with the seismic influence coefficient curve used by the mode shape decomposition response spectrum method in a statistical sense. When three sets of acceleration time history curves are input, the calculation result should take the envelope value of the time history method.

Considering the spectral characteristics of ground motion, the predominant period of the selected seismic wave is as consistent as possible with the design characteristic period, and the epicentral distance of the selected seismic wave is as consistent as possible with that of the proposed site. The design conditions of site Class II, the design earthquake group is the second group, the seismic fortification intensity is 8 degrees, and the design basic acceleration is 0.3g are taken as an example. Natural

seismic waves El-centro, Taft, and artificial RH4TG040 are selected. Figure 5 shows that the seismic wave response spectrum curves after amplitude modulation is in agreement with the design response spectrum curve and the average seismic wave response spectrum curve. If the seismic fortification intensity is 8 degrees, for the spatial grid structure such as the single-layer reticulated shell structure, the vertical seismic effects should be checked [31, 32].

The traveling wave effect of seismic waves could act on the large-span spatial roof structures [33]. However, it is difficult to define the minimum span that needs to consider the traveling wave effect. GB 50011-2010 [32] stipulates that large-span spatial structures with specific plane projection size, including structures with span greater than 120 m, length greater than 300 m, or cantilever greater than 40 m, shall consider the traveling wave effect. According to the seismic response analysis of single-layer cylindrical latticed shells and square pyramid latticed frames by scholars, the traveling wave effect should be considered when the structure length exceeds 200 m [34]. Since the span of the models in this paper is 60 meters, the traveling wave effect is not very significant. The consistent input method is adopted for seismic wave input. The influence of other input methods on the seismic response of the single-layer reticulated shells will be studied separately in the future.



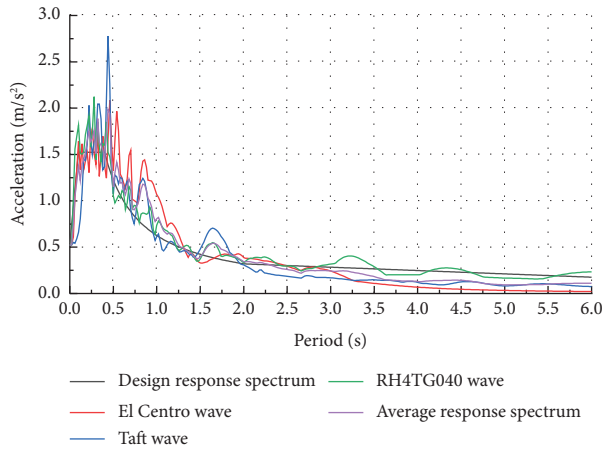


FIGURE 5: Response spectrum curves.

### 3. Results and Discussion

**3.1. Influence on Dynamic Characteristics.** The first 80 natural vibration frequencies and modes of both the simplified models and the flexibly suspended models. In the simplified models, the CHS is simplified as fixed masses on the suspension nodes, as shown in Figure 2. The vibration modes and frequencies of the simplified models and the flexibly suspended models are compared, and the influence of the sling length and the CHS weight on the vibration modes and frequencies is discussed.

**3.1.1. Influence on the Vibration Modes.** Table 2 shows that the first two modes of the simplified model are antisymmetric with vertical deformation, and the third mode is symmetric with main vertical deformation. The reason is that the vertical stiffness is far less than the horizontal stiffness. It is displayed that when the CHS is flexibly suspended, the first three modes are the horizontal swing of the CHS, and the fourth to sixth modes are the torsion of the CHS itself, and the seventh mode is the vertical mode with the coupling of the CHS and the reticulated shell. The only tension feature of the slings leads to the horizontal swing or torsion of the CHS. The frequency of the first three modes of the flexibly suspended model is significantly lower than that of the simplified model. This is because the horizontal constraint of the CHS is low, so the first three vibration modes are mainly the rigid body displacement of the CHS. It is shown that the flexibly suspended model is divided into two parts due to the use of slings. The modes of the overall structure show the motion of the CHS itself and the mode of coupling effect.

**3.1.2. Influence on Vibration Frequencies.** Figure 6 shows that when the CHS is simplified to fixed masses, the first three natural frequencies decrease along with the increase in the weight  $w$  of the CHS. This is because increasing the weight of the CHS is equivalent to increasing the mass of the overall structure, but there is no obvious change in the

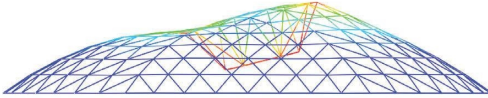
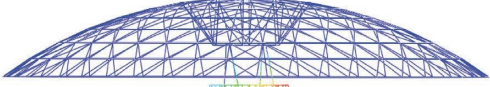
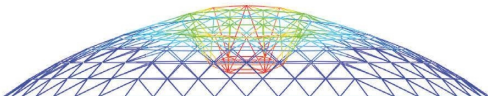
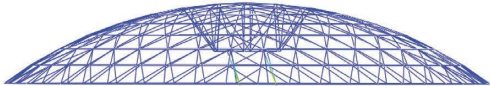
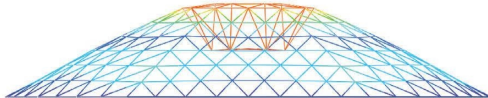
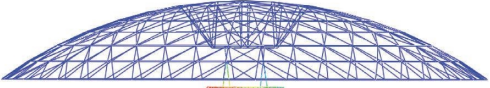
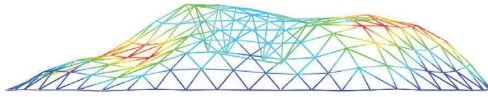

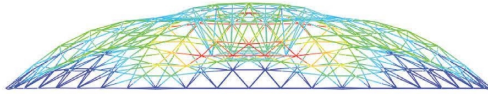

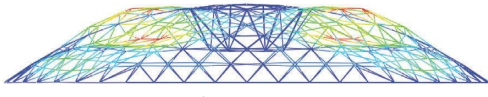

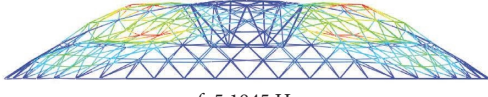
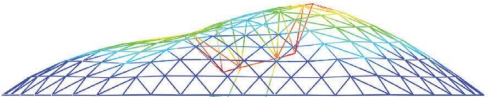
structural stiffness. From the fourth mode onwards, the weight has little effect on the natural frequency of the simplified model. For the flexibly suspended models, the frequencies under different sling lengths  $l$  show similar laws. Figure 7 shows that the weight has little influence on the first three numbers of natural frequencies, but has a significant influence on the fourth to the thirteenth numbers, and has little influence on higher numbers. The 4<sup>th</sup> to 13<sup>th</sup> modes show the interaction between the CHS and reticulated shell, which is greatly affected by the CHS. The 14<sup>th</sup> and higher numbers are mainly the vibration mode of the lattice shell itself, which is less affected by the concentrated mass of the CHS. The results show that the influence of the CHS weight on the natural frequency of the flexibly suspended models is obvious. In general, the weight has little influence on the high numbers natural frequency, but has a greater influence on the low numbers natural frequency.

Figures 8 and 9 show the curves of the natural frequencies varying with the sling length under  $w = 20$  t and  $w = 40$  t, respectively. It is shown that the influence rules of the sling length are the same under different CHS weights. Furthermore, the natural frequencies of the simplified model ( $l = 0$  m) are higher than those of the flexibly suspended model ( $l > 0$  m) from the top 80 numbers of frequencies. Compared with the simplified model, the first three natural frequencies of the flexibly suspended model are significantly reduced, but the first three natural frequencies are basically the same under different sling lengths. This is because the first three vibration modes are mainly the free swing of the CHS. The results show that the influence of the sling length on the natural frequencies is obvious, especially, it has a greater impact on some low numbers natural frequencies, while it has no effect on the high numbers natural frequencies.

**3.2. Influence on Seismic Responses.** The influence on the axial forces of the reticulated shell members is mainly concerned since underestimation on the internal forces could affect the structural safety. The axial forces and nodal acceleration of the flexibly suspended cases and the simplified cases are compared. The introduction of the acceleration reveals the relationship between motion and force to a certain extent, and it is convenient to evaluate the seismic response of local part of the shell. The degree that the axial forces are affected, the position of the most affected members are analysed. The deep mechanisms by which the CHS affects seismic responses under vertical seismic motions are discussed based on both axial forces and nodal acceleration. The influence laws of the sling length and the scoreboard weight on the seismic responses are also discussed.

**3.2.1. Influence on Axial Forces.** The envelope peak values of the time history of axial forces under three sets of seismic waves are taken as the peak axial force of a structural member. The symbol  $F_{j,\max}^{w,l}$  is set as the peak axial force of

TABLE 2: Modes and frequencies of simplified models and flexibly suspended models.

Mode number	The simplified models	The flexibly suspended models
1	 $f=3.6525$ Hz	 $f= 0.0000$ Hz
2	 $f=3.7142$ Hz	 $f=0.0000$ Hz
3	 $f=4.2984$ Hz	 $f=0.0000$ Hz
4	 $f=4.9439$ Hz	 $f=2.6504$ Hz
5	 $f=4.9511$ Hz	 $f=2.9464$ Hz
6	 $f=5.0835$ Hz	 $f=3.4246$ Hz
7	 $f=5.1845$ Hz	 $f=4.3401$ Hz

the  $j$  th member when the weight of the CHS is  $w$  and the sling length is  $l$ , where  $j$  is a positive integer. Then, the change rate  $\gamma_{j,\max}^{w,l}$  of the  $j$  th member can be obtained by equation (1), where the symbol  $F_{j,\max}^{w,0}$  represents the peak axial force when the weight of the CHS is  $w$  and the CHS is simplified as fixed

masses on the support platform. The maximum change rate  $\gamma_{\max}^{w,l}$  of the axial forces of the single-layer reticulated shell members is calculated, by equation (2), for analysing the degree of the influence of  $w$  and  $l$  on the axial forces of all members, where  $p$  is the total number of members in the shell.

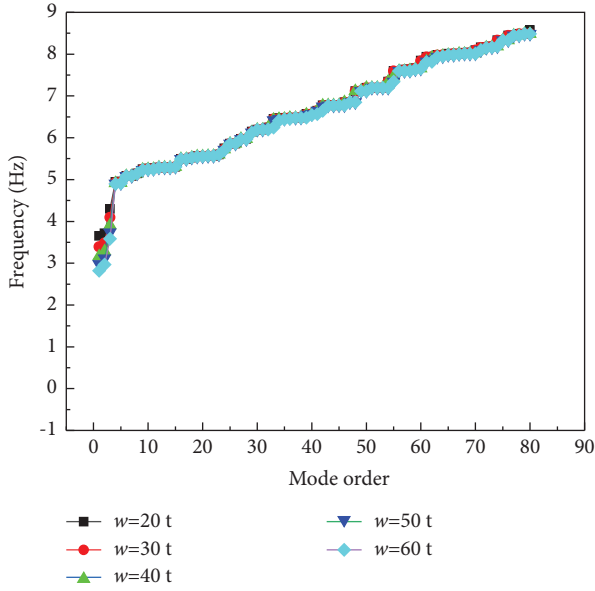


FIGURE 6: Frequencies of the simplified models.

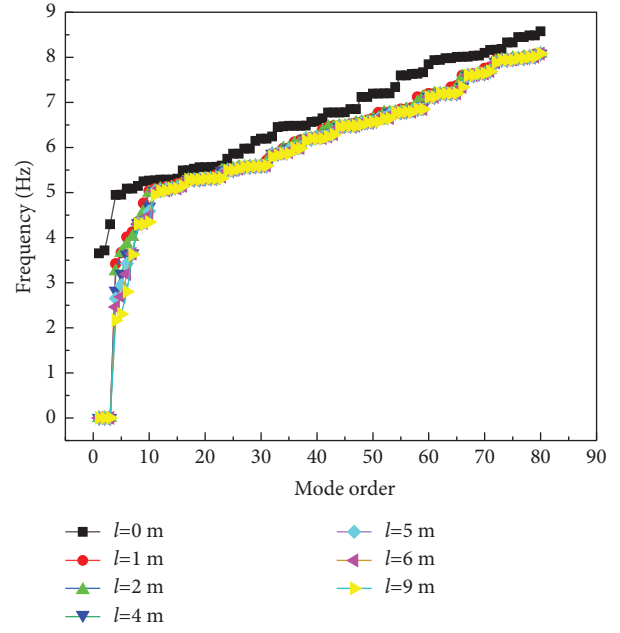


FIGURE 8: Frequencies of the models ( $w = 20$  t).

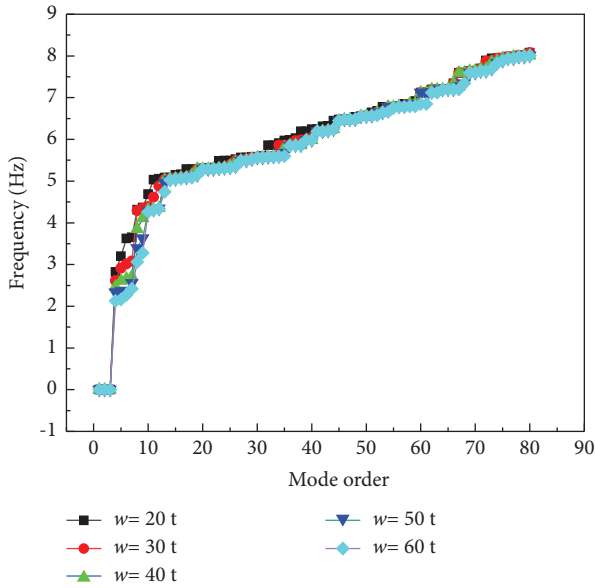


FIGURE 7: Frequencies of the flexibly suspended models ( $l = 4$  m).

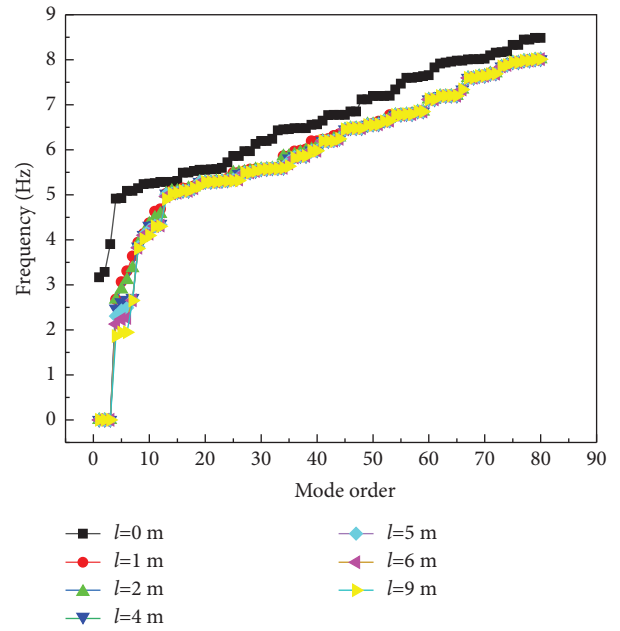


FIGURE 9: Frequencies of the models ( $w = 40$  t).

$$\gamma_{j,\max}^{w,l} = \frac{F_{j,\max}^{w,l} - F_{j,\max}^{w,0}}{F_{j,\max}^{w,0}}, \quad (1)$$

$$\gamma_{\max}^{w,l} = \max_{j=1 \sim p} \{ \gamma_{j,\max}^{w,l} \}. \quad (2)$$

Figure 10 shows that the  $\gamma_{\max}^{w,l}$  values of shell members are between 46.9% and 130.4%. Figure 11 shows that the  $\gamma_{\max}^{w,l}$  values of support platform members are between 6% and 532.0%. It shows that the axial forces of some members on the shell and on the platform in the flexibly suspended model could increase by up to 1.3 times and 5.32 times of those in the simplified model. It indicates that the amplification effect

of the CHS on the axial forces of the shell members and the platform members are significant, and axial forces could be underestimated if a simplified model is used for analysis subjected to vertical seismic motions. The deep reason is that the different dynamic characteristics between the CHS and the structure result in the vertical impact effect on the structure under vertical seismic motions.

Figure 10 shows that the maximum  $\gamma_{\max}^{w,l}$  value appears when the weight is 30 t and the sling length is 1 m. When the weight is less than 40 t, the  $\gamma_{\max}^{w,l}$  value of the reticulated shell

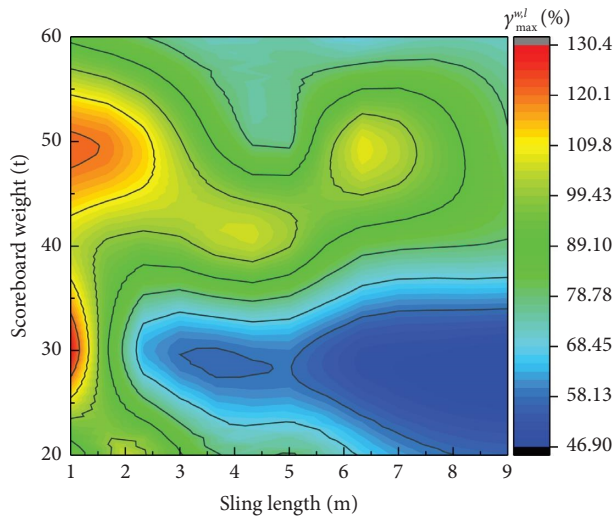


FIGURE 10: The  $\gamma_{\max}^{w,l}$  values of shell members.

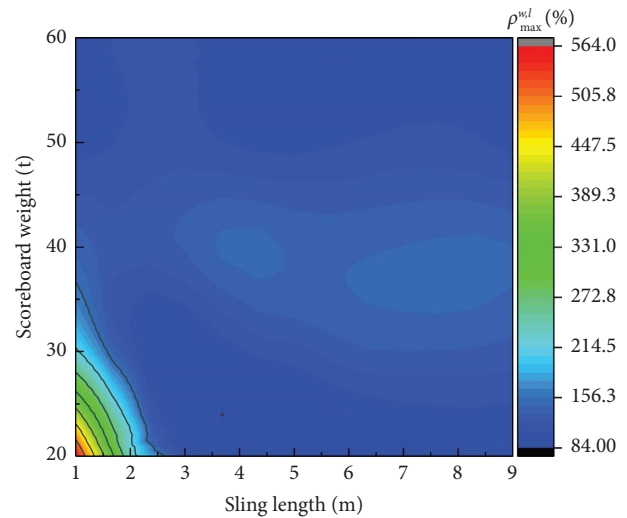


FIGURE 12: The  $\rho_{\max}^{w,l}$  values of shell nodes.

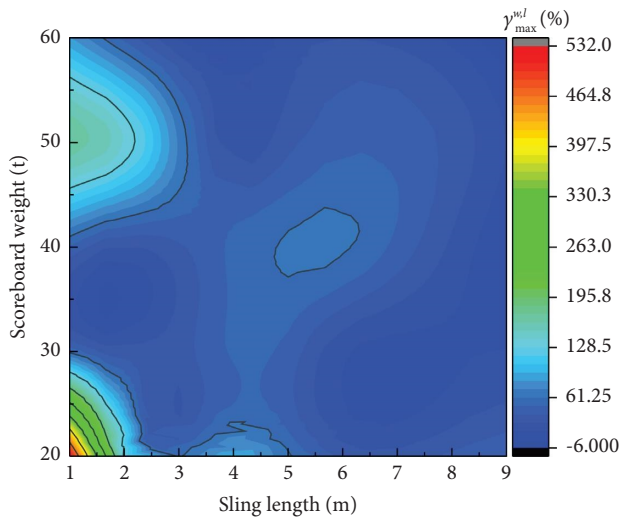


FIGURE 11: The  $\gamma_{\max}^{w,l}$  values of support platform members.

members gradually decreases with the increase in the sling length. When the sling length is greater than 2.5 m, the  $\gamma_{\max}^{w,l}$  value of the shell members is not significantly affected by the weight. Figure 11 shows that the maximum  $\gamma_{\max}^{w,l}$  value appears when the weight is 20 t and the sling length is 1 m. When the sling length is less than 3 m, the  $\gamma_{\max}^{w,l}$  value of the platform members decreases first and then increases with the increase of the weight. The  $\gamma_{\max}^{w,l}$  value of the platform members reaches a local peak when the weight is 50 t and the sling length is 1 m. When the sling length is greater than 3 m, the  $\gamma_{\max}^{w,l}$  value of the platform members is less affected by the weight and the sling length, and the  $\gamma_{\max}^{w,l}$  value is maintained below 70%. Generally, the influence laws of the weight and the sling length on axial forces under vertical seismic motions are complicated. The deep reason is that the dynamic characteristics of the integrated structure are significantly influenced by the weight and the sling length. However, Figures 10 and 11 show only overall degree of the influence

of the CHS on the axial forces of the shell members with the variation of the weight and the length. The position of the most affected members needs to be displayed and discussed.

### 3.2.2. The Position of the Most Affected Members.

Contours and peak axial force change rates  $\gamma_{\max}^{w,l}$  of structural members are displayed in Table 3, so as to illustrate the position of the most affected members. It shows that when the sling length is 1 m and 2 m, the  $\gamma_{j,\max}^{w,l}$  value of the central part of the reticulated shell is greater than that near the boundary. As the length of the sling increases, the  $\gamma_{j,\max}^{w,l}$  value of the reticulated shell member gradually decreases as a whole. It is displayed that the hoop members have significantly larger  $\gamma_{j,\max}^{w,l}$  value than other shell members. For the platform members, it is shown that the  $\gamma_{j,\max}^{w,l}$  value of all is quite high in some cases. It indicates that hoop members and members in the center region of the reticulated shell are the most affected members, and all members of the platform are the most affected members.

The platform members are directly connected with the CHS, and the vertical impact effect affects the platform members first. The same theory can explain the most affected region of the center part of the shell. But there are two reasons why the hoop members are most affected members. The first and main reason is that the acceleration of the relevant nodes increases significantly, which is illustrated in Section 3.3, under vertical seismic motions. The second is that the cross-sections of hoop members are controlled by slenderness, and the axial forces of hoop members are very low. Then, the  $\gamma_{j,\max}^{w,l}$  values of hoop members are sensitive to the increase of axial forces.

It is also displayed that the parameters  $w$  and  $l$  significantly affect the distribution of change rate  $\gamma_{j,\max}^{w,l}$  of the reticulated shell members and the platform members, but the influence laws are complicated. There are many types of single-layer reticulated shells, and the shells of one type are usually unique with different parameters in practice. It is hard to find a general rule for all single-layer reticulated shells. It is suggested that axial forces of the structural



TABLE 3: Contours and peak axial force change rates  $\gamma_{max}^{wl}$  of structural members.

Length (m)	Weight				
	20 t	30 t	40 t	50 t	60 t
1					
	$\gamma_{max}^{wl} = 83.2\%$	$\gamma_{max}^{wl} = 130.3\%$	$\gamma_{max}^{wl} = 104.6\%$	$\gamma_{max}^{wl} = 121.4\%$	$\gamma_{max}^{wl} = 86.9\%$
	$\gamma_{max}^{wl} = 531.4\%$	$\gamma_{max}^{wl} = 56.9\%$	$\gamma_{max}^{wl} = 48.5\%$	$\gamma_{max}^{wl} = 169.6\%$	$\gamma_{max}^{wl} = 84.7\%$
2					
	$\gamma_{max}^{wl} = 105.6\%$	$\gamma_{max}^{wl} = 70.9\%$	$\gamma_{max}^{wl} = 95.8\%$	$\gamma_{max}^{wl} = 117.3\%$	$\gamma_{max}^{wl} = 81.1\%$
	$\gamma_{max}^{wl} = 123.1\%$	$\gamma_{max}^{wl} = 36.0\%$	$\gamma_{max}^{wl} = 26.0\%$	$\gamma_{max}^{wl} = 144.2\%$	$\gamma_{max}^{wl} = 45.8\%$
4					
	$\gamma_{max}^{wl} = 75.2\%$	$\gamma_{max}^{wl} = 57.9\%$	$\gamma_{max}^{wl} = 105\%$	$\gamma_{max}^{wl} = 81.9\%$	$\gamma_{max}^{wl} = 71.3\%$
	$\gamma_{max}^{wl} = 97.6\%$	$\gamma_{max}^{wl} = 54.4\%$	$\gamma_{max}^{wl} = 52.9\%$	$\gamma_{max}^{wl} = 17.5\%$	$\gamma_{max}^{wl} = 1.1\%$
5					
	$\gamma_{max}^{wl} = 80.2\%$	$\gamma_{max}^{wl} = 59.8\%$	$\gamma_{max}^{wl} = 99.9\%$	$\gamma_{max}^{wl} = 76.4\%$	$\gamma_{max}^{wl} = 75.6\%$
	$\gamma_{max}^{wl} = 63.5\%$	$\gamma_{max}^{wl} = 46.7\%$	$\gamma_{max}^{wl} = 63.3\%$	$\gamma_{max}^{wl} = 36.1\%$	$\gamma_{max}^{wl} = 21.5\%$
6					
	$\gamma_{max}^{wl} = 70.6\%$	$\gamma_{max}^{wl} = 52.0\%$	$\gamma_{max}^{wl} = 84.2\%$	$\gamma_{max}^{wl} = 105.8\%$	$\gamma_{max}^{wl} = 68.2\%$
	$\gamma_{max}^{wl} = 34.8\%$	$\gamma_{max}^{wl} = 17.2\%$	$\gamma_{max}^{wl} = 64.5\%$	$\gamma_{max}^{wl} = 47.2\%$	$\gamma_{max}^{wl} = 27.7\%$

TABLE 3: Continued.

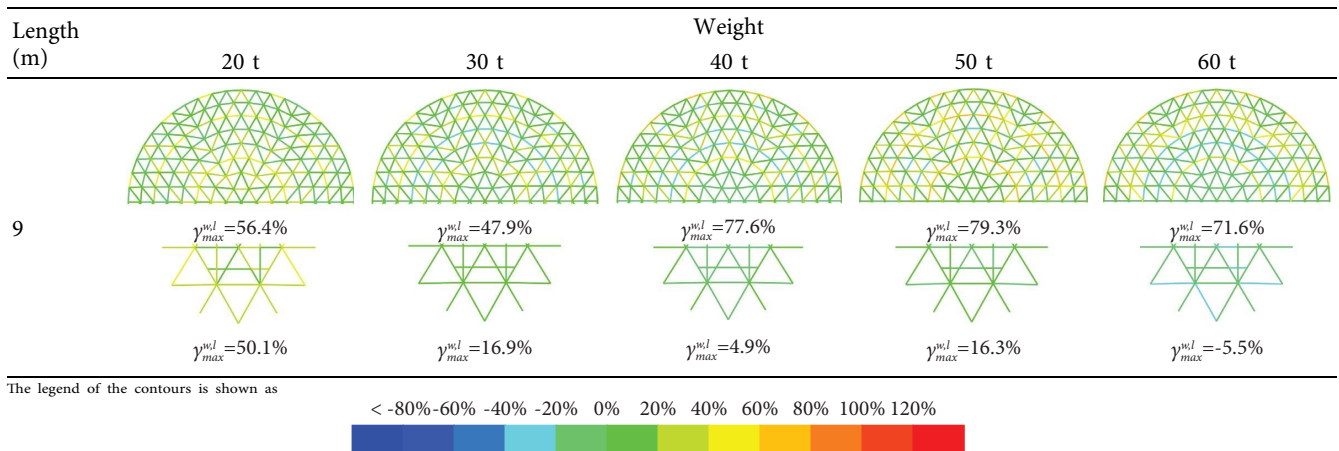


TABLE 4: Contours and peak acceleration change rates  $\rho_{max}^{wl}$  of the nodes.

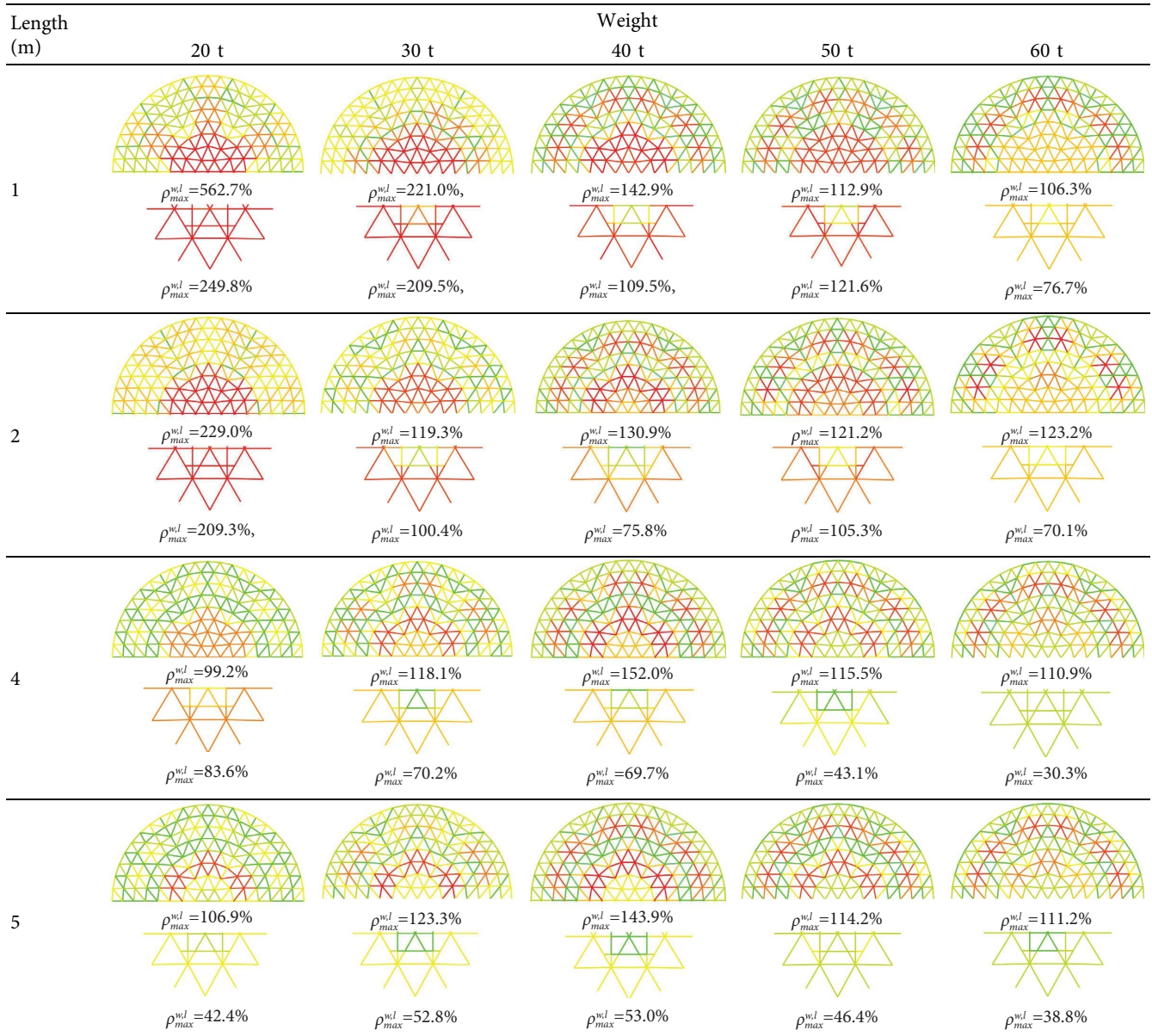
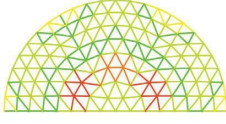
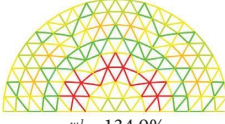






















TABLE 4: Continued.

Length (m)	Weight				
	20 t	30 t	40 t	50 t	60 t
6	 $\rho_{max}^{w,l} = 101.9\%$	 $\rho_{max}^{w,l} = 134.9\%$	 $\rho_{max}^{w,l} = 144.5\%$	 $\rho_{max}^{w,l} = 117.1\%$	 $\rho_{max}^{w,l} = 105.2\%$
	 $\rho_{max}^{w,l} = 38.0\%$	 $\rho_{max}^{w,l} = 45.6\%$	 $\rho_{max}^{w,l} = 45.8\%$	 $\rho_{max}^{w,l} = 65.6\%$	 $\rho_{max}^{w,l} = 29.1\%$
9	 $\rho_{max}^{w,l} = 106.7\%$	 $\rho_{max}^{w,l} = 132.8\%$	 $\rho_{max}^{w,l} = 147.0\%$	 $\rho_{max}^{w,l} = 114.1\%$	 $\rho_{max}^{w,l} = 110.4\%$
	 $\rho_{max}^{w,l} = 38.3\%$	 $\rho_{max}^{w,l} = 31.6\%$	 $\rho_{max}^{w,l} = 31.9\%$	 $\rho_{max}^{w,l} = 27.5\%$	 $\rho_{max}^{w,l} = 11.3\%$

The legend of the contours is shown as.

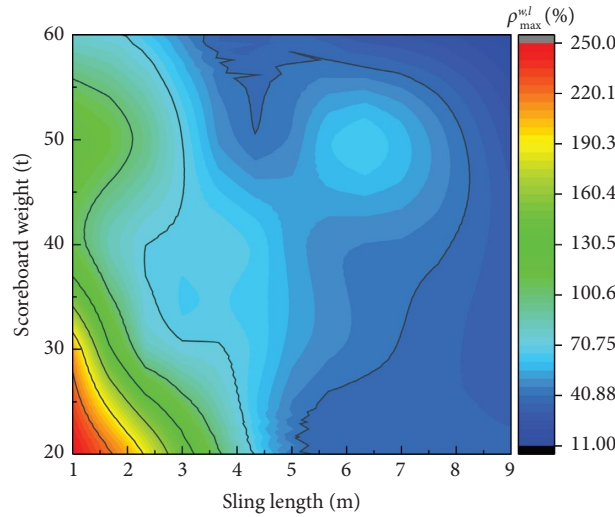
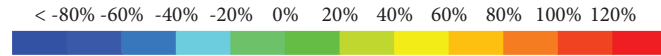


FIGURE 13: The  $\rho_{max}^{w,l}$  values of support platform nodes.

members, considering all possible lengths under seismic motions should be used for design of cross-sections of the members.

3.3. Influence on Nodal Acceleration. With the same theory for numbering the change rate of axial forces, the acceleration of the  $i$  th node on the reticulated shells is set as  $a_{i,max}^{w,l}$ , and the peak acceleration change rate of the  $i$ -th node is  $\rho_{i,max}^{w,l}$  (equation (3)). The  $\rho_{max}^{w,l}$  values (equation (4)) of the

reticulated shells and the platform members are displayed in Table 4. The parameter  $n$  is the number of the structural members.

$$\rho_{i,max}^{w,l} = \frac{a_{i,max}^{w,l} - a_{i,max}^{w,0}}{a_{i,max}^{w,0}}, \quad (3)$$

$$\rho_{max}^{w,l} = \max_{i=1 \sim n} \{ \rho_{i,max}^{w,l} \}. \quad (4)$$

Figure 12 shows that the  $\rho_{\max}^{w,l}$  values of the reticulated shell nodes are between 84% and 564%. Figure 13 displays that the  $\rho_{\max}^{w,l}$  values of the support platform nodes are between 11% and 250%. It indicates that the CHS significantly influences the acceleration of the structure under the action of vertical seismic, and the acceleration could be underestimated if the CHS is simplified as fixed masses on the suspension nodes. The maximum  $\rho_{\max}^{w,l}$  values of both the shell nodes and the platform nodes occur when the weight is 20 t and the sling length is 1 m. With the increase of the weight and the sling length, the  $\rho_{\max}^{w,l}$  value of the shell nodes decreases suddenly. When the weight is more than 30 t and the sling length is more than 2.5 m, the weight and the sling length have little influence on the  $\rho_{\max}^{w,l}$  value. With the increase of the weight and the sling length, the  $\rho_{\max}^{w,l}$  value of the platform nodes also shows a complicated decrease trend. However, Figures 12 and 13 show only the overall degree of the influence of the CHS on the acceleration of the nodes with the variation of the weight and the length. The position of the most affected nodes needs to be displayed and discussed.

Contours and peak acceleration change rates  $\rho_{\max}^{w,l}$  of nodes are displayed in Table 4, so as to show the position of the most affected nodes. It is shown that the most affected nodes are located at two regions, one is the central part of the shell and another is the third hoops of the shell. It is also shown that all the platform nodes are significantly affected. The distribution of the most affected node acceleration is consistent with the position of the most affected axial forces. This is due to the vertical impact effect of the CHS under the vertical seismic motions.

#### 4. Conclusions

In this paper, the seismic responses on the SPRS with a CHS under vertical seismic motions are investigated. The dynamic characteristics and seismic responses of the flexibly suspended models and the simplified models are analysed and compared in the Abaqus software. The influence of the weight and the sling length of the CHS on the seismic response of the SPRS is also discussed.

- (1) Under different CHS weight and the sling length, the first three vibration modes are all free swing of the CHS, and the CHS weight and the sling length have a significant impact on the fourth and subsequent vibration modes. Compared with the simplified model, the first three natural frequencies of the flexibly suspended model are significantly reduced. The length of the sling only has a large impact on some low numbers natural frequencies, but has little impact on the high numbers natural frequencies.
- (2) Compared with the simplified model, the axial forces of some structural members and some nodal acceleration in the flexibly suspended under vertical seismic motions would increase by as high as 523% and 564%, respectively. It turns out that the seismic responses of the SPRS would be underestimated if a simplified model is used for analysis.

- (3) The parameters including the weight of the CHS and the sling length significantly affect the distribution of peak axial force change rate of the reticulated shell members and the distribution of peak acceleration change rate, but the influence laws are complicated.
- (4) The region in the central of the SPRS, the hoop members of the SPRS, and the support platform are the most affected regions in terms of both axial force and nodal acceleration. This is due to the vertical impact effect of the CHS.
- (5) The envelope results of the flexibly suspended cases taking different CHS weights and sling lengths into account are recommended for structural design. But if a simplified model is used, the most affected regions must be concerned and strengthened.
- (6) The weight of the CHS is usually determined by the owner of the gym. If the weight is determined, it is suggested that the vertical location of the CHS when it is not being used is quite important. Because the sling length has a significant effect on the seismic response. Since every gym is different, the best location should be studied case by case.

#### Data Availability

No data has been used in the article.

#### Conflicts of Interest

The authors declare that they have no conflicts of interest regarding the publication of this paper.

#### Acknowledgments

This study was funded by the Natural Science Foundation of Shandong (ZR201911030049).

#### References

- [1] H. H. Ma, Y. Y. Ma, F. Fan, and Y. N. Zhang, "Seismic performance of single-layer spherical reticulated shells considering joint stiffness and bearing capacity," *Advanced Steel Construction*, vol. 18, no. 02, pp. 604–616, 2022.
- [2] W. L. Li, X. D. Zhi, and F. Fan, "Influence of the roofing system on the seismic performance of single-layer spherical reticulated shell structures," *Buildings*, vol. 12, no. 155, 2022.
- [3] Z. Cao and Y. G. Zhang, "Analysis of seismic response characteristics of single layer spherical reticulated shells," *Building Structures*, vol. 8, pp. 195–201, 1998.
- [4] J. H. Lin, Y. Zhang, and Y. Zhao, "Seismic analysis methods of long-span structures and recent advances," *Advances in Mechanics*, vol. 31, no. 03, pp. 350–360, 2001.
- [5] S. Z. Shen and X. D. Zhi, "Failure mechanism of reticulated shells subjected to dynamic actions," *China, Civil Engineering Journal*, vol. 38, no. 01, pp. 11–20, 2005.
- [6] K. Ishikawa, S. Okubo, Y. Hiyama, and S. Kato, "Evaluation method for predicting dynamic collapse of double layer latticed space truss structures due to earthquake motion," *International Journal of Space Structures*, vol. 15, no. 3, pp. 249–257, 2000.

- [7] S. Kato, T. Ueki, and Y. Mukaiyama, "Study of dynamic collapse of single layer reticular domes subjected to earthquake motion and the estimation of statically equivalent seismic forces," *International Journal of Space Structures*, vol. 12, no. 3-4, pp. 191-203, 1997.
- [8] K. Ishikawa and S. Kato, "Elastic-plastic dynamic buckling analysis of reticular domes subjected to earthquake motion," *International Journal of Space Structures*, vol. 12, no. 3-4, pp. 205-215, 1997.
- [9] S. D. Xue, Y. G. Zhang, Z. Cao, and X. Y. Li, "Prospect and further development of seismic research and spatial structures over last thirty years in China," *Industrial Construction*, vol. 43, no. 06, pp. 105-116, 2016.
- [10] F. Fan, M. L. Wang, Z. G. Cao, and S. Shen, "Seismic behaviour and seismic design of single-layer reticulated shells with semi-rigid joint system," *Advances in Structural Engineering*, vol. 15, no. 10, pp. 1829-1841, 2012.
- [11] H. H. Ma, Z. W. Shan, and F. Fan, "Dynamic behaviour and seismic design method of a single-layer reticulated shell with semi-rigid joints," *Thin-Walled Structures*, vol. 119, pp. 544-557, 2017.
- [12] C. Wang and S. Z. Shen, "Dynamic stability of single layer reticulated dome under step load," *Advances in Steel Structures*, vol. 1, pp. 201-208, 1999.
- [13] W. F. Du, B. Q. Gao, and S. L. Dong, "Elastic-plastic dynamic stability of single-layer reticulated domes considering damage accumulation," *Space structures*, vol. 15, no. 02, pp. 35-38, 2009.
- [14] W. J. Zhang, L. H. Xu, and Y. G. Zhang, "Study on strong earthquake failure mechanism and parameter influence of single-layer spherical reticulated shell," *World Earthquake Engineering*, vol. 35, no. 03, pp. 1-9, 2019.
- [15] J. Zhong, X. D. Zhi, and F. Fan, "Analyses of seismic fragility of single-layer cylindrical reticulated shells under near-fault and far-field ground motions," *China Civil Engineering Journal*, vol. 53, no. S2, pp. 177-182, 2020.
- [16] Z. W. Yu, X. D. Zhi, F. Fan, and C. Lu, "Effect of substructures upon failure behavior of steel reticulated domes subjected to the severe earthquake," *Thin-Walled Structures*, vol. 49, no. 9, pp. 1160-1170, 2011.
- [17] M. Zhang, J. Y. Hou, X. D. Zhi, and W. L. Li, "Effect of initial geometric imperfection modes on seismic performance of single-layer spherical reticulated shell," *Journal of Vibration and Shock*, vol. 40, no. 05, pp. 33-38+74, 2021.
- [18] T. L. Zhang, Y. Ding, and Z. X. Li, "Study on the influence of initial geometric defects on the seismic bearing capacity of single-layer spherical reticulated shell structure," *Spatial Structure*, vol. 24, no. 03, pp. 3-9, 2018.
- [19] J. Zhang, H. Li, and C. Li, "Seismic response of large-span spatial structures under multi-support and multidimensional excitations including rotational components," *Earthquake Engineering and Engineering Vibration*, vol. 20, no. 1, pp. 141-159, 2021.
- [20] Y. Z. Zhou, *Shaking Table Tests and Performance Study of Single-Layer Reticulated Cylindrical Shells with Skin Diaphragm*, Master Thesis, Beijing University of Technology, Beijing, China, 2012.
- [21] L. S. Huo, Y. W. Zhang, C. Huang, and H. N. Li, "Research on vibration control of large-span spatial structures with a passive adaptive suspended mass pendulum," *Journal of Disaster Prevention and Mitigation Engineering*, vol. 41, no. 5, pp. 968-976, 2021.
- [22] X. F. Cai, H. Yu, and C. Nan, "Discussion on design of center-hung scoreboard system for large arena," *Electrical Technology of Intelligent Buildings*, vol. 12, no. 05, pp. 92-98+5, 2018.
- [23] W. Z. Hao, J. Q. Wang, and Q. Li, "Introduction to the center-hung display scheme of a provincial gymnasium," *Video Engineering*, vol. 43, no. 05, pp. 23-25+45, 2019.
- [24] S. D. Xue, Z. T. Zhao, X. Y. Li et al., "Shaking table test research on the influence of center-hung scoreboard on natural vibration characteristics and seismic response of suspen-dome structures," *Buildings*, vol. 12, no. 8, p. 1231, 2022.
- [25] S. D. Xue, Z. Lu, X. Y. Li et al., "Experimental and numerical investigations on the influence of center-hung scoreboard on dynamic characteristics of suspend-dome structure," *Journal of Building Engineering*, vol. 57, Article ID 104787, 2022.
- [26] R. J. Liu, C. Wang, and G. Y. Wang, "Analysis of natural vibration characteristics of single layer spherical reticulated shell structure with flexible suspended bucket screen," *Building Structures*, vol. 51, no. s2, pp. 360-365, 2021.
- [27] Y. F. Luo, Y. Xiang, and Z. Y. Shen, "Research and application status of seismic analysis techniques for large-span spatial structures," *Chinese Quarterly of Mechanics*, vol. 36, no. 1, pp. 1-10, 2015.
- [28] B. Ehforooz, P. Memarzadeh, and F. Behnamfar, "Evaluating the conventional pushover procedures for estimating the seismic performance of steel plate shear walls," *Journal of Civil Engineering and Urbanism*, vol. 4, no. 1, pp. 19-27, 2014.
- [29] M. Fallahi, S. S. Roudsari, T. M. Abu-Lebdeh, and F. I. T. Petrescu, "Investigating the effects of frp bars on the seismic behavior of reinforced concrete coupling beams," *Independent Journal of Management & Production*, vol. 10, no. 8, pp. 1819-1833, 2019.
- [30] S. Sundar, B. K. Bhagavan, and A. Datta, "Computing eigenvalues: Lanczos algorithm with a new recursive partitioning method," *Computers & Mathematics with Applications*, vol. 38, no. 5-6, pp. 99-107, 1999.
- [31] Chinese Standard, *Technical Specification for Space Frame Structures: JGJ 7-2010*, China Architecture & Building Press, Beijing, China, 2010.
- [32] Chinese Standard, *Code for Seismic Design of Buildings: GB50011-2010*, China Architecture & Building Press, Beijing, China, 2010.
- [33] Q. J. Wang, Z. Zeng, J. F. Zhang, and S. Q. Zhang, "The seismic analysis of large-span spatial structures considering the traveling wave effects," *Earthquake resistant engineering and Retrofitting*, vol. 40, no. 4, pp. 59-63, 2018.
- [34] T. Su, N. B. Qin, and T. Z. Wang, "Seismic response analysis of super-long latticed shell structure," *Journal of Hefei Union University*, vol. 37, no. 2, pp. 80-88, 2015.